Three-dimensional numerical simulations of cellular jet diffusion flames

C. E. Frouzakis[a,*], A. G. Tomboulides[b], P. Papas[c], P. F. Fischer[d], R. M. Rais[a], P. A. Monkewitz[e], K. Boulouchos[a]

[a] *Aerothermochemistry and Combustion Systems Laboratory*
Swiss Federal Institute of Technology Zurich (ETHZ)
CH-8092 Zurich, Switzerland
[b] *Department of Energy Resources Management and Engineering*
Aristotle University of Thessaloniki, 50100 Kozani, Greece
[c] *Division of Engineering*
Colorado School of Mines, Golden CO 80401, USA
[d] *Mathematics and Computer Science Division*
Argonne National Laboratory, Argonne IL 60439, USA
[e] *Fluid Mechanics Laboratory*
Swiss Federal Institute of Technology Lausanne (EPFL)
CH-1015 Lausanne, Switzerland

Abstract

Recent experimental investigations have demonstrated that the appearance of particular cellular states in circular non-premixed jet flames depends significantly on a number of parameters, including the initial mixture strength, reactant Lewis numbers, and proximity to the extinction limit (Damköhler number). For CO_2-diluted H_2/O_2 jet diffusion flames, these studies have shown that a variety of different cellular patterns or states can form. For given fuel and oxidizer compositions, several preferred states were found to co-exist, and the particular state realized was determined by the initial conditions. In order to elucidate the dynamics of cellular instabilities, circular non-premixed jet flames are modeled with a combination of three-dimensional numerical simulation and linear stability analysis (LSA). In both formulations, chemistry is described by a single-step, finite-rate reaction, and different reactant Lewis numbers and molecular weights are specified. The three-dimensional numerical simulations show that different cellular flames can be obtained close to extinction and that different states co-exist for the same parameter values. Similar to the experiments, the behavior of the cell structures is sensitive to (numerical) noise. During the transient blow-off process, the flame undergoes transitions to structures with different numbers of cells, while the flame edge close to the nozzle oscillates in the streamwise direction. For conditions similar to the experiments discussed, the LSA results reveal various cellular instabilities, typically with azimuthal wavenumber $m = 1 - 6$. Consistent with previous theoretical work, the propensity for the cellular instabilities is shown to increase with decreasing reactant Lewis number and Damköhler number.

Keywords:Cellular flame, diffusion flame instability

1. Introduction

Experimental evidence dating back many decades [1] has shown that cellular instabilities exist for gaseous diffusion flames. The experiments of Chen *et al.* [2] clearly demonstrated the importance of relatively low Lewis and Damköhler numbers on the occurrence of cellularity in Wolfhard-Parker burner flames. More recent experimental work on cell formation in non-premixed axisymmetric jet flames, identified the variety of spatio-temporal patterns forming near the extinction limit [3]. In addition to the importance of low reactant Lewis numbers, these experiments demonstrated the importance of the initial mixture strength [3, 4], with the propensity for cellularity increasing with decreasing initial mixture strength. The initial mixture strength is defined here as the ratio of the fuel mass fraction supplied in the fuel stream to the oxidizer mass fraction supplied in the oxidizer stream normalized by the stoichiometric ratio.

For premixed flames, many studies can be found in the literature that deal with cell formation in circular burners. These patterns include uniformly rotating ring(s) of cells [5], and ratcheting or chaotic motions [6]. Theoretical studies [7] have well established that the formation of cellular structures in premixed flames arises from thermo-diffusive instabilities that occur when a weighted Lewis number is sufficiently low [7]. Since three-dimensional numerical simulations have been too expensive in the past, simple phenomenological models have been developed to replicate the cellular patterns [8].

Recent theoretical work has shown that the formation of cellular structures in diffusion flames can also be attributed to thermo-diffusive instabilities [9–11]. The stability analysis performed by Cheatham and Matalon [10], for example, demonstrated that the propensity for the formation of cellularity increases with increasing heat loss and decreasing reactant Lewis numbers, Damköhler number, and initial mixture strength. Numerical simulations of counterflow diffusion flames have also demonstrated that transitions from cellular states with narrow "stripes" to wider "stripes" occur as the Damköhler number is reduced [12].

Cell formation in non-premixed circular jet flames involves a large number of physical effects and parameters; consequently, both experimental and numerical information will be required to elucidate the underlying physics. Such information is still incomplete. For example, the dynamics and types of cellular patterns as well as the parameter space in which these different cell patterns develop in non-premixed flames have not been fully investigated. The current study investigates cellular instabilities occurring in non-premixed circular jet flames near the extinction limit. In order to elucidate the physics behind recent experimental findings [3, 4], three-dimensional numerical simulations have been undertaken in combination with linear stability analysis.

In this paper, we start with a brief review of the recent experimental investigations into cell formation in circular jet flames near extinction. We then present the results obtained with three-dimensional numerical simulations of the experimental system. Finally, we briefly discuss the results from a linear stability analysis, elucidating the influence of the reactant Lewis numbers and the Damköhler number on the different azimuthal modes near extinction.

2. Experimental observations

A recent publication [3] reported a systematic experimental investigation of cell formation in CO_2-diluted H_2-O_2 circular jet non-premixed flames. Since numerical simulations of these experiments are the focus here, a brief description of some results from this publication will be given. The EPFL jet flame facility [3, 13] consists of a free jet apparatus, oriented vertically up and mounted on a precision traverse, together with PC-based data acquisition and control systems. An intensified CCD camera with 14-bit resolution was used to record images of the streamwise integrated chemiluminescence emission from above the flame tip. The flow rates of the hydrogen, oxygen, and (diluent) carbon dioxide gases to the jet apparatus were set with fully automated flow controllers. The gaseous fuel passed through a muffler, a settling chamber with honeycomb straighteners and screens, and finally through a contoured axisymmetric contraction with an area ratio of 100:1. The diameter of the circular fuel nozzle was $D = 0.75$ cm. A uniform co-flow of a O_2-CO_2 mixture was introduced through a porous plate of 7.5 cm diameter surrounding the fuel nozzle. The uniform fuel velocity was $U_F = 76$ cm/s, and the co-flowing oxidizer stream velocity, U_O, was fixed at 4 cm/s.

The parameter space near the extinction limit was investigated by fixing the fuel composition (H_2-CO_2 mixture) and then systematically lowering the O_2 concentration in the co-flowing O_2-CO_2 stream. The O_2 concentration was lowered in decrements of less than 0.1% (by volume) until a transition to cellular flames was first observed, and then further until the extinction limit was reached. The conditions for these near-extinction experiments covered a range of reactant Lewis numbers, based on the *overall fuel-oxygen mixture* at 300 K of $[1.1\text{-}1.2]$ for oxygen and $[0.25\text{-}0.29]$ for hydrogen, and initial mixture strength ϕ_m from $0.08 - 1.34$.

Figure 1 shows the various types of cellular modes observed at a fixed jet fuel composition (22.5% vol. H_2, except for the last image (f) observed for 21.5% H_2) and various oxygen concentrations above the extinction limit of 23.2% O_2. These images were taken from above the flame, and the false-color scale is related to the intensity of the chemiluminescence, integrated in the streamwise direction over the entire length of the flame. In the terminology of [5], the cellular states in these images are classified by the number of cells, followed by the letters "R" or "S" for rotating and stationary states, respectively. When

visualized in the dark laboratory with the naked eye, all these flames revealed distinctively cellular flame structures that varied little in the streamwise direction. The flame height for these flames was less than three jet diameters.

The experiments showed that cellular flames occur near the extinction limit, and the parameter space for cellularity was found to increase with decreasing initial mixture strength. For fixed initial fuel and oxygen concentrations in their respective reactant streams, several cellular states were found to co-exist, and the particular state realized was determined by the initial conditions and the path adopted in parameter space to reach the experimental condition. Mode switching could also be induced by suitable perturbations such as noise, transient perturbations of the jet flow field, or introduction of bluff bodies at the jet exit. With all other conditions fixed, the transitions between cellular flames with different number of cells were also studied for a 22.5% H_2-77.5% CO_2 fuel mixture. The composition of the oxidizer stream was carefully varied between 35% and the extinction value of 23.2% O_2. Within this range, hysteretic transitions between flames with one to five cells were observed, and the range of oxidizer compositions over which the different flame structures were stable was identified. The number of cells in the preferred states observed was found to decrease with decreasing oxygen concentration (Damköhler number).

3. Numerical simulations

3.1. Problem formulation

The conservation equations of mass, momentum, species and energy in the low Mach number limit were integrated with a parallel, spectral-element based code. The spectral element method is a high-order weighted residual technique that couples the efficiency of global spectral methods with the geometric flexibility of finite elements methods. Locally, the mesh is structured, with the data and geometry expressed as sums of Nth-order tensor product polynomials [14]. Globally, the mesh is an unstructured array of deformed hexahedral elements. Temporal discretization is based on a second-order, operator-splitting formulation for low speed compressible reacting flows that permits large time steps.

The code uses scalable domain-decomposition-based iterative solvers with efficient preconditioners. The parallel implementation is based on the standard message-passing Single Program Multiple Data (SPMD) mode, where contiguous groups of elements are distributed to processors and the computation proceeds in a loosely synchronous manner; communication is based on the MPI standard. More information about the numerical algorithms can be found in [14–17]. The code exhibits very good parallel efficiency and scalability properties, sustaining high MFLOPS, on a number of distributed-memory platforms.

The computational domain was a cylinder with diameter equal to five times the jet diameter, D=0.75 cm, and height equal to $10D$. The fuel stream was CO_2-diluted H_2 ($X_{H_2}^{fuel} = 0.215$) that enters the domain with a top-hat velocity profile of $U_F = 76$ cm/s at T=300K. The oxidizer was a O_2-CO_2 mixture ($X_{O_2}^{ox} = 0.50$), with a uniform velocity profile of $U_O = 4$ cm/s, and T=300K. To avoid numerical discontinuities, the exit velocity profiles were approximated by a steep hyperbolic tangent profile (see description in the linear analysis section). For the species, flux (mixed) boundary conditions (BC) were used on the nozzle plane, and zero-Neumann BC on the rest of the domain boundaries. On the outer cylinder boundary, the slip wall BC with axial velocity equal to U_O was used for the momentum, and fixed-temperature BC for the energy. On the outflow boundary, zero normal stress BC were used for the momentum equation, and zero-Neumann BC for the rest of the variables. Although the temperature variation of the transport properties was taken into account, the non-dimensional parameters Reynolds, Re, Prandtl, Pr, and Lewis, Le_i, were kept fixed at $Re = 517$, $Pr = 0.52$, $Le_{H_2} = 0.26$, $Le_{O_2} = 1.15$, $Le_{H_2O} = 1.12$, and $Le_{CO_2} = 1.7$. These values were calculated with the Chemkin [18] routines, using as reference quantities the properties of the overall fuel-oxidizer mixture. Other reference variables used in the non-dimensionalization were $T_{ref} = T_F = 300$ K, $U_{ref} = U_F$, and $t_{ref} = D/U_F = 9.9$ ms. The chemistry was described by a single-step reaction, $2H_2 + O_2 \rightarrow H_2O$, with reaction rate expression $r = A\ T^n\ \exp(-T_a/T)\ [H_2]^2\ [O_2]$. The reaction rate parameters were taken from [19] as $n = 0.91$, T_a=27.7 , and the dimensionless heat of reaction was equal to ΔH_r=44.12. The initial non-dimensional pre-exponential factor was $A = 1.33 \cdot 10^9$. Theoretical and stability analysis of diffusion flames usually employ a Damköhler number that includes the exponential term at the 'adiabatic flame temperature' and the initial fuel and oxidizer mass fractions (e.g. [10]). A similar approach was adopted in the experiment, where the Damköhler number was changed by modifying the initial composition of the oxidizer stream.

In the simulations, the pre-exponential factor was directly lowered to bring the system close to the extinction limit. Two grids were employed with 1166 and 2376 elements and interpolating polynomial orders of $6 \leq N \leq 8$ and $N = 4$ in each of the three spatial directions, respectively. The largest simulation had a total of about 600,000 points, corresponding to more than 5 million unknowns. All computations were performed on a 64-CPU Linux cluster.

3.2. Numerical results

For the conditions described above, the initial value $A = 1.33 \cdot 10^9$ resulted in a stable flame without cells that was anchored at the nozzle. The factor A was then lowered until flame extinction was observed for $A = 1.7 \cdot 10^8$. Extinction in this case

corresponded to blow-off as the flame was lifted from the jet exit. In all cases considered ($1.7 \cdot 10^8 < A < 1.33 \cdot 10^9$), the fuel was fully consumed in the numerical domain, and the flame was lifted from the jet exit. Cells at the edge of the flame close to the jet exit appeared at $A = 5 \cdot 10^8$ and persisted all the way down to extinction. The lifted edge of the flame was no longer at the same height at different locations along the azimuthal direction but attained a wavy structure. The high-temperature regions with the cell-like structure did not persist all the way to the outflow. Overall, cellular flames with 6-, 4-, 3- and 2-cell structures were observed (Fig. 2). The 6-cell structure was obtained for $A = 3 \cdot 10^8$, whereas 4-cell and fewer cell structures were obtained for $A \leq 2.5 \cdot 10^8$. It was found that, similar to the experiments, the transition to the different cellular flames is sensitive to (numerical) noise. In some cases, this noise was enough to produce an unsteady solution (periodic with very small amplitude and low frequency) and in other cases to cause a transition from one state to another. The 2-cell structures were observed only during the transient extinction process of the flame at $A = 1.7 \cdot 10^8$, described below. We note that the symmetry of the obtained structures is not related to the symmetry of the computational grid (which was four fold for the 1166-element grid and eight fold for the 2376-element grid, i.e. the grids were divided into four or eight sections in the azimuthal direction).

3.3. Flame structure

The structure of the 4-cell flame was analyzed by extracting the temperature, species, reaction rate and mixture fraction profiles along one-dimensional cuts at different flame heights. The mixture fraction was defined as $\xi = sY_{\mathrm{H}_2} - Y_{\mathrm{O}_2} + Y_{\mathrm{O}_2}^{ox}/(sY_{\mathrm{H}_2}^{fuel} + Y_{\mathrm{O}_2}^{ox})$, where $s = \nu_{\mathrm{H}_2} W_{\mathrm{H}_2}/(\nu_{\mathrm{O}_2} W_{\mathrm{O}_2}) = 8$ is the mass stoichiometric ratio, and W_i represent species molecular weights. The stoichiometric mixture fraction for these conditions was then $\xi_{\mathrm{st}} = 1/(1 + sY_{\mathrm{H}_2}^{fuel}/Y_{\mathrm{O}_2}^{ox}) = 0.809$. Despite the unequal Lewis numbers, the diffusion flame was, to a good approximation, located close to the stoichiometric mixture fraction surface [10]. At $A = 1.8 \cdot 10^8$, the diffusion flame was lifted from the nozzle exit. The isocontours of the reaction rate (Fig. 2(g)) show a triple flame structure, with a weak diffusion flame tail located around the stoichiometric mixture fraction isoline plotted with the dot-dashed line. The heights where the flame structure was extracted are indicated by the solid lines marked "1", "2", and "3" at z=1.0, z=3.0, and z=3.5, respectively, and the corresponding flame structures are plotted in Fig. 4(a-c).

For the profiles at z=1.0, significant leakage of fuel and oxidizer through the reaction zone can be observed, and the flame has an essentially premixed character (the fuel-rich branch of the triple flame). At z=3.0 and z=3.5, the significantly lower reaction rate profile acquired a second peak associated with the diffusion flame tail, while the first peak was from the fuel-lean premixed flame branch of the triple flame.

Similar to the experiment, co-existence of two different cellular structures was observed at the same parameter values. Figures 2(a) and 2(b) show the stationary 3- and 4-cell flame computed for $A = 1.8 \cdot 10^8$. The 4-cell flame was obtained first with the 1166-element simulation for polynomial order $N = 8$. The result was then interpolated onto a 2376-element grid with $N = 4$ (corresponding, overall, to a lower resolution because of the lower order of the interpolating polynomials). The integration of the conservation equations with the interpolated fields as initial condition, resulted, after the initial transient, in a flame with three cells. In other words, the numerical noise introduced by the interpolation and the lower resolution was enough to perturb the system to the stationary 3-cell state. The resulting fields were then interpolated back to the high-resolution grid; the 3-cell state remained stable, obviously showing that it is also a stable flame structure for $A = 1.8 \cdot 10^8$. The co-existence of two stable steady states at the same parameter values shows that the hysteretic transition between different cellular structures observed experimentally is also reproduced by the simulations.

3.4. Flame extinction

Starting with the 4-cell state for $A = 1.8 \cdot 10^8$ as initial condition, the pre-exponential factor was reduced to $A = 1.7 \cdot 10^8$. The flame went through a sequence of transitions with different number of cells (the 4-, 3-, and 2-cell flames observed are shown in Fig. 3), while the edge of the flame close to the nozzle oscillated with a growing amplitude. Eventually, the flame blew off. The four-cell flames persisted for a long time from the start of the calculation (about 200 non-dimensional units). During this period, two of the four cells located opposite from each other had higher temperature, reaction rate and size than the other two. The pair of cells burning stronger changed from upper-left/lower-right (Fig. 3(a)) to upper-right/lower-left (Fig. 3(b)). The maximum temperature and the flame height (determined from the location where the temperature was twice that of the inlet streams) during the extinction process are plotted in Fig. 5; both variables oscillated as the flame blew off.

3.5. Stability analysis

To elucidate the stability characteristics for axisymmetric flames, a viscous linear stability analysis was employed using a finite rate, one-step reaction model. A brief description will be given below. Details about the axisymmetric jet flame analysis can be found in [20, 21]. A similar methodology was also followed in a recent publication considering the instabilities of *planar* diffusion flames [11].

The *undisturbed basic state* considered is a reacting axisymmetric jet surrounded by a co-flowing ox-

idizer stream –a diffusion flame formed between two parallel streams of hydrogen-water and oxygen. Unless otherwise indicated, the parameters chosen to model this flame are specified in the *Problem formulation* section. The mean profiles were taken to be frozen in the streamwise direction (parallel flow assumption). The mean velocity profile was represented with a hyperbolic tangent profile [22]: $U = 0.5\{1 + tanh[0.25(R/\theta)(R/r - r/R]\}$, where R is the jet radius and θ the momentum thickness. The mean temperature and mean mass fractions were determined using a methodology discussed in [11, 21].

The linearized continuity, momentum, energy, species, and state equations, including reaction and diffusion terms, were obtained with the following assumptions: body forces (e.g. gravity) and bulk viscosity were neglected; the flow was assumed to be low subsonic; the multi-component gas mixture properties (thermal conductivity, specific heat at constant pressure, and viscosity) were assumed equal for all species (unity Prandtl numbers); the mass diffusion coefficients (defined by Fick's law) were assumed equal to the binary mass diffusivity of all species pairs. Finally, the terms in the energy equation due to viscous stresses, radiative heat transfer, interdiffusion, and the Dufour effect were neglected. As in the formulation for the numerical simulations, the non-dimensionalization of the governing equations was based on the reference quantities of the fuel stream. The viscosity μ, thermal conductivity λ, and density-weighted mass diffusivity (ρD) were all assumed to follow Chapman's law ($\mu = \lambda = \rho D_i = T$ in non-dimensional form). Different Lewis numbers $\mathrm{Le}_i = \lambda_0/c_{p,0}(\rho D_i)$ were specified for the reactants, with the subscript 0 denoting properties of the fuel stream at $r = 0$.

Once the basic state was computed, temporal stability computations were performed. The perturbations were in the form of normal modes $q'(r, x, \phi, t) = \hat{q}(r) \exp\ i(\alpha x + m\phi - \omega t)$, where ω is the complex frequency, m the azimuthal wave number, and α the complex wave number. The resulting eigenvalue problem was solved with a shooting method, starting the numerical integration from both sides of the mixing layer with asymptotic solutions valid for vanishing radial gradients of the base flow.

Although not all parameters of the three-dimensional simulations were matched, most of the parameters used in the stability analysis correspond closely to the simulations. Similar to the numerical simulations, $R/\theta = 20$ was chosen which has been shown to correspond to experimental conditions [20]. The far-field temperatures of both reactant streams were taken to be equal. The initial mixture strength ϕ_m and the Reynolds number were fixed at 0.5 and 500, respectively. Finally, the finite-rate hydrogen-oxygen reaction was characterized by a non-dimensional activation energy $T_a = 30$, normalized by the fuel free stream temperature. The molecular weights for hydrogen and product were taken to be 2 and 18, respectively, and the quiescent oxidizer stream was chosen to be pure oxygen. Also, the appropriate heat release parameter was chosen to obtain a maximum (normalized with the fuel centerline temperature) temperature $T_{\max} = 6.0$ at the flame-sheet limit for unity Lewis numbers (cf. Ref. [11]).

Temporal stability calculations were performed for this *representative* H_2-O_2 flame over a range in Damköhler number, Da, close to its extinction limit, $\mathrm{Da_E}$. The fuel and oxidizer Lewis numbers were fixed at $\mathrm{Le_{H_2}} = 0.3$ and $\mathrm{Le_{O_2}} = 1.0$, respectively. Figure 6 shows the maximum temporal growth rate $\omega_{i,\max}$ as a function of Da for the azimuthal modes $m = 1 - 6$. The figure reveals several interesting features. First, the different azimuthal modes become unstable over different and overlapping intervals of the Damköhler number just prior to the extinction limit at $\mathrm{Da_E} = 1.098 \times 10^{-3}$. Second, the respective maximum growth rates of each azimuthal mode $m = 1 - 6$ are relatively close, and progressively increase with decreasing Da. The Da value where a particular azimuthal mode first becomes unstable is designated as $\mathrm{Da_*(m)}$, and corresponds to $\mathrm{Da_*(m)} = 2.49,\ 2.45,\ 2.42,\ 2.10,\ 1.90$, and 1.80×10^{-3} for the $m = 1,\ 2,\ 3,\ 4,\ 5$, and 6 modes, respectively. A plot of $\omega_{i,\max}$ as a function of $\mathrm{Da} - \mathrm{Da_*(m)}$ is shown in the upper right-hand corner of Fig. 6, where the different $\mathrm{Da_*(m)}$ values for the azimuthal modes are specified above. Figure 6 illustrates that the dominant mode changes with Damköhler number, and the $m = 1$ mode is dominant just prior to the extinction condition.

4. Conclusions

With single-step chemistry and constant but unequal reactant Lewis numbers, the three-dimensional simulation of a CO_2-diluted H_2 jet diffusion flame showed cell flame structures similar to the ones observed experimentally. Flames with different numbers of cells were obtained close to extinction. The transient extinction process itself showed transitions to cellular states containing different number of cells. These transient flame structures oscillated in various ways, and the entire flame eventually blew off. Similar to the experiments, the cellular states were found to be sensitive to noise, which was enough to lead from a 4- to a 3-cell flame structure for the same parameter values. This coexistence of different cellular flames was also observed experimentally. The cellular flames were found to be associated with a large leakage of reactants through the reaction zone, and exhibit a triple flame structure at the flame base near the jet exit.

Given the simplifications of a linear stability analysis, comparisons between experiments, as well as direct numerical simulations, can only be qualitative; however, linear stability theory has provided many insights into the physics behind cell formation. Previous research [9, 10] on thermo-diffusive instabilities in non-premixed flames has shown that both reactant Lewis numbers, $\mathrm{Le_F}$ and $\mathrm{Le_O}$, are important parame-

ters. At Damköhler numbers near the extinction limit, cellular instabilities for axisymmetric jet flames have been shown to be dominant at relatively low Lewis numbers, while axisymmetric pulsations can dominate at relatively high Lewis numbers [21]. For a representative H_2-O_2 jet diffusion flame, the linear stability results reported here show that multiple azimuthal modes, which become destabilized near the extinction limit, have comparable growth rates for a given Damköhler number. The overlapping intervals in Damköhler number where these unstable modes appear is consistent with the co-existence of multiple states observed both in the experiments and the numerical simulations near the extinction limit. For the conditions of this study, the linear stability calculations [21] also indicate that the various azimuthal modes, which are thermo-diffusive instabilities, are absolute instabilities; however, further work will be required to elucidate their relevance to actual flame dynamics. Currently, numerical work is underway to identify the range of parameter values over which the different flame structures are stable, and study the transition between these different structures.

Acknowledgments

The financial support from the Swiss Office of Energy (BfE) for CEF and KB, the Swiss National Science Foundation (grants NF20-61887.00 and NF-57100.99) for PP and RMR, a SNSF grant (number PIOI2-103091) for AGT, and from the U.S. Department of Energy (Contract W-31-109-Eng-38) for PFF is gratefully acknowledged. The authors are also grateful to Prof. M. Matalon for many fruitful discussions.

References

[1] J.E. Garside, B. Jackson, *Nature* **168** (1951), 1085.
[2] R.-H. Chen, G.B. Mitchell, P.D. Ronney, *Proc. Combust. Inst.* **24** (1992) 213–221.
[3] D. Lo Jacono, P. Papas, P.A. Monkewitz, *Combust. Theory Modelling* **7** (2003) 634–644.
[4] M. Füri, Non-premixed jet flame instabilities, Ph.D. thesis no. 2468, Swiss Federal Institute of Technology Lausanne (EPFL), (2001).
[5] M. Gorman, F. Hamill, M. el-Hamdi, K.A. Robbins, *Combust. Sci. Tech.* **98** (1994) 25–35.
[6] M. Gorman, M. el-Hamdi, B. Pearson, K.A. Robbins, *Physical Review Letters* **76**(2) (1996) 228–231.
[7] P. Clavin P *Prog. Energy Combust. Sci.* **11** (1985) 1–59.
[8] A. Palacios, G.H. Gunaratne, M. Gorman, K.A. Robbins, *Chaos* **7**(3) (1997) 463–475.
[9] J.S. Kim, *Combust. Theory Modelling* **1** (1997) 13–40.
[10] S. Cheatham, M. Matalon *J. Fluid Mech.* **414** (2000) 105–144.
[11] P. Papas, R.M. Rais, A.G. Tomboulides, P.A. Monkewitz, *Combust. Theory Modelling* **7** (2003), 603–633.
[12] S.R. Lee, J.S. Kim, *Combust. Theory Modelling* **6** (2002) 263–278.
[13] M. Füri, P. Papas, P.A. Monkewitz, *Proc. Combust. Inst.* **28** (2000) 831–838.
[14] M.O. Deville, P.F. Fischer, E.H. Mund, *High-Order Methods for Incompressible Fluid Flow.* Cambridge University Press, 2002.
[15] P.F. Fischer, H.M. Tufo, in *Parallel Computational Fluid Dynamics: Towards Teraflops, Optimization and Novel Formulations.* D. Keyes, A. Ecer, N. Satofuka, P. Fox, and J. Periaux (eds.) North-Holland, 2000, p. 17-26.
[16] A.G. Tomboulides, J. Lee, S. A. Orszag, *J. Sci. Comp.*, **12**(2) (1997) 139–167.
[17] A.G. Tomboulides, and S.A Orszag, *J. Comp. Phys.*, **146**(2), 691–706, (1998).
[18] R.J. Kee, G. Dixon-Lewis, J. Warnatz, M.E. Coltrin, J.A. Miller, *A Fortran Computer Code for Evaluation of Gas-Phase Multicomponent Transport Properties*, Report No. SAND86-8246, Sandia National Laboratories, 1986.
[19] A. Beccantini, H. Paillére, R. Morel, F. Dabbene, 17th International Colloquium on the Dynamics of Explosions and Reactive Systems, July 25-30, 1999, Heidelberg, Germany.
[20] M. Füri, P. Papas, R.M. Rais, P.A. Monkewitz, *Proc. Combust. Inst.* **29** (2002) 1653–1661.
[21] R.M. Rais. Investigations of diffusion flame instabilities, PhD thesis no. 2700, Swiss Federal Institute of Technology Lausanne (EPFL), (2002).
[22] A. Michalke, *Prog. Aerospace Sci.* **21**:159-199 (1984).

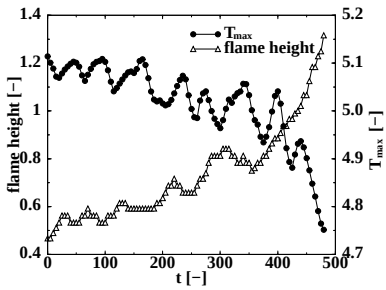

Fig. 5: Maximum flame temperature and flame height during the transient extinction process

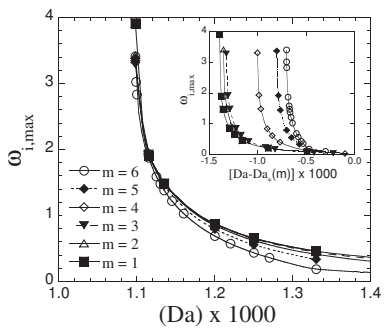

Fig. 6: Maximum temporal growth rate $\omega_{i,\max}$ as a function of the Damköhler number Da for the different azimuthal wave numbers $m = 1 - 6$. The results for $m = 0$ are not shown.

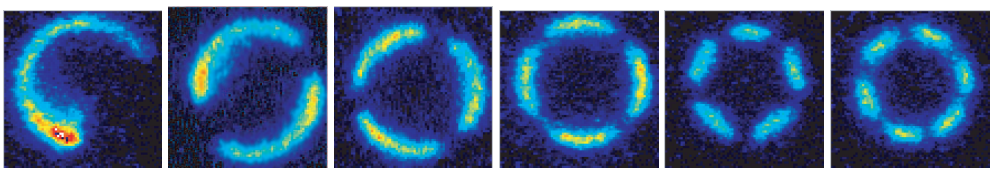

(a) 1R-cell (b) 2R-cell (c) 3R-cell (d) 4S-cell (e) 5S-cell (f) 6S-cell

Fig. 1: Streamwise integrated chemiluminescence images taken from the downstream jet axis of a 22.5% H_2 (78.5% CO_2) jet flame burning in (a) 24.6% O_2 (75.4% CO_2) co-flow; (b) 26.0% O_2 co-flow; (c) 27.5% O_2 co-flow; (d) 31.0% O_2 co-flow, (e) 40.0% O_2 co-flow, and (f) 21.5% H_2 (79.5% CO_2) jet flame burning in 70.0% O_2 co-flow. "R" designates rotating and "S" stationary cell patterns. Fuel centerline and oxidizer velocities are $U_F = 76$ and $U_O = 4$ cm/s, respectively. [Figs. (a)-(e) taken with permission from Ref. [3]]

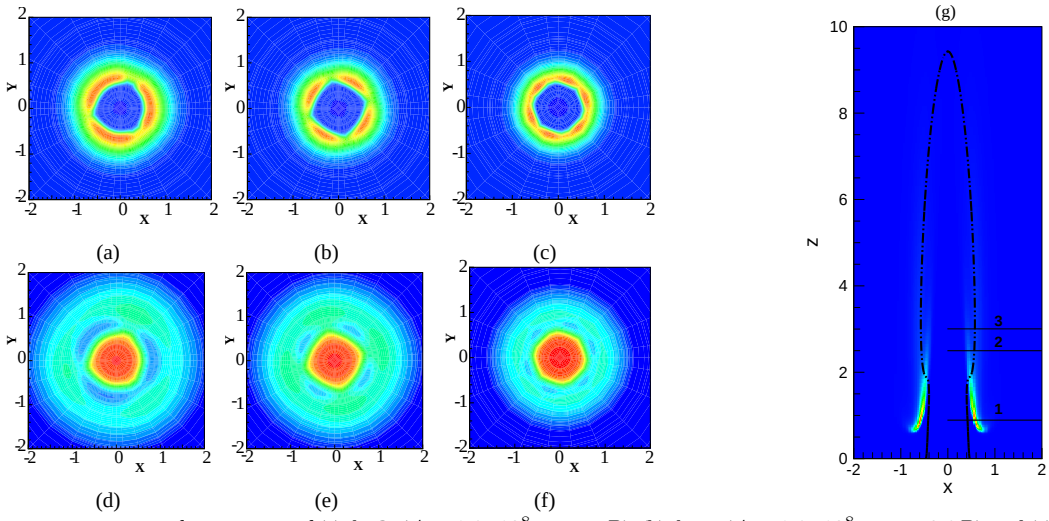

Fig. 2: Isocontours of temperature of (a) the 3- ($A = 1.8 \cdot 10^8$, at $z = D$), (b) the 4- ($A = 1.8 \cdot 10^8$, at $z = 0.8D$), and (c) the 6-cell flame ($A = 2.5 \cdot 10^8$, at $z = 0.5D$); (d)-(f) corresponding fuel mass fraction; (g) heat release rate for the 4-cell flame. Scales are from blue (low) to red (high): $1 \leq T \leq 5$, $10^{-4} \leq Y_F \leq 1.2 \cdot 10^{-2}$, and $0 \leq$ reaction rate ≤ 0.12.

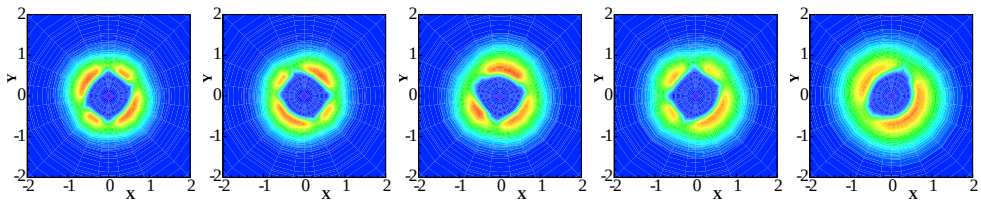

(a) (b) (c) (d) (e)

Fig. 3: Temperature isocontours showing the different cell structures observed during flame blow off for $A = 1.7 \cdot 10^8$ (from left to right: t=100, 165, 340, 445, 480 non-dimensional time units, at heights 0.9, 0.95, 1.3, 1.5, and 2.0 nozzle diameters, respectively). Scales are from blue (low) to red (high): $1 \leq T \leq 5$.

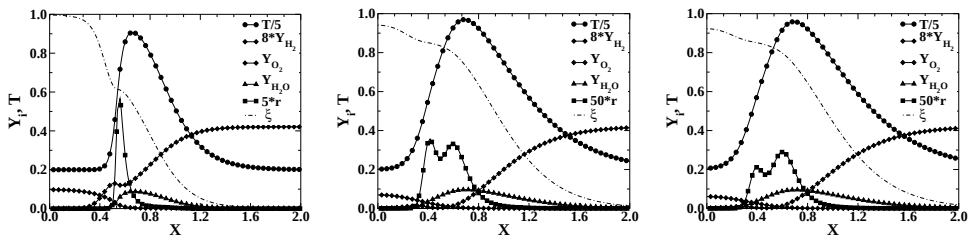

(a) (b) (c)

Fig. 4: Flame structure of the 4-cell flame at (a) z=1.0, (b) z=5.0, and (c) z=3.5 ($A = 1.8 \cdot 10^8$).